January 2020

A Classification Of Ice Crystal Habits Using Combined CPL And RSP Observations During The Seac4rs Campaign

Natalie Midzak

A CLASSIFICATION OF ICE CRYSTAL HABITS USING COMBINED CPL AND RSP OBERVATIONS DURING THE SEAC^{4}RS CAMPAIGN

by

Natalie Midzak
Bachelor of Science, Millersville University, 2017

A Thesis

Submitted to the Graduate Faculty

of the

University of North Dakota

in partial fulfillment of the requirements

for the degree of

Master of Science

Grand Forks, North Dakota

May 2020

This thesis submitted by Natalie Midzak in partial fulfillment of the requirements for the Degree of Master of Science from the University of North Dakota, has been read by the Faculty Advisory Committee under whom the work has been done and is hereby approved.

Jianglong Zhang

John Yorks

Aaron Kennedy

This thesis is being submitted by the appointed advisory committee as having met all of the requirements of the School of Graduate Studies at the University of North Dakota and is hereby approved.

Chris Nelson
Dean of the School of Graduate Studies

Date

PERMISSION

Title A Classification of Ice Crystal Habits Using Combined CPL and RSP Observations During the Seac^{4}rs Campaign

Department Atmospheric Sciences

Degree Master of Science

In presenting this thesis in partial fulfillment of the requirements for a graduate degree from the University of North Dakota, I agree that the library of this University shall make it freely available for inspection. I further agree that permission for extensive copying for scholarly purposes may be granted by the professor who supervised my thesis work or, in her absence, by the Chairperson of the department or the dean of the School of Graduate Studies. It is understood that any copying or publication or other use of this thesis or part thereof for financial gain shall not be allowed without my written permission. It is also understood that due recognition shall be given to me and to the University of North Dakota in any scholarly use which may be made of any material in my thesis.

Natalie Midzak
May 3, 2020

Table of Contents

List of Figures

List of Tables

ACKNOWLEDGMENTS

I wish to express my sincere appreciation to my advisor, Dr. Jianglong Zhang, my mentor, Dr. John Yorks, and committee member, Dr. Aaron Kennedy, for their guidance and support during my time in the master's program at the University of North Dakota. I would also like to thank my collaborators, Dr. Bastiaan van Diedenhoven and Dr. Sarah Woods for their contributions to this research. Finally, I would like to thank my family, especially my Baba, for teaching me the importance of education and always encouraging me to work hard.

ABSTRACT

Using collocated NASA's Cloud Physics Lidar (CPL) and Research Scanning Polarimeter (RSP) data from the SEAC^{4}RS campaign, a new observational-based method was developed which uses a K-means clustering technique to classify ice crystal habit types into seven categories: column, plates, rosettes, spheroids and three different type of irregulars. Inter-compared with the collocated SPEC Inc. Cloud Particle Imager (CPI) data, the frequency of the detected ice crystal habits from the proposed method presented in the study agree within 5% of the CPI reported values for columns, irregulars, rosettes, and spheroids, with more disagreement for plates. This study suggests that a detailed ice crystal habit retrieval could be applied to combined space-based lidar and polarimeter observations such as CALIPSO and POLDER in addition to future missions such as the Aerosols, Clouds, Convection, and Precipitation (A-CCP).

CHAPTER I

INTRODUCTION

Cirrus clouds consistently cover almost half of the Earth's surface and impact the global climate system through their role in the radiative budget (Mace et al. 2009; Wylie and Menzel 1999). Cirrus can either warm or cool the atmosphere depending on the height, particle properties, and optical thickness of the cirrus cloud. While cirrus cloud heights and optical thickness can be measured from space-based remote sensing (Campbell et al. 2015; Holz et al. 2016), cirrus microphysical properties remain a major uncertainty in determining their radiative impacts despite the high frequency of cirrus. Given this uncertainty, studies using radiative forcing models generally assume a random orientation of hexagonal planar or columnar ice crystals, which are only the building blocks to more intricate habits (Figure 1). This simplified assumption leads to inaccuracies in the estimation of cirrus radiative impacts. A main source of ice cloud radiative forcing error stems from scattering parameters of the varying ice crystal habits (Zhang et al. 1999; Wendisch et al. 2005). A better understanding of cirrus microphysical properties, especially the shape and size of ice crystals, is necessary to more accurately quantify their effects on the climate system.

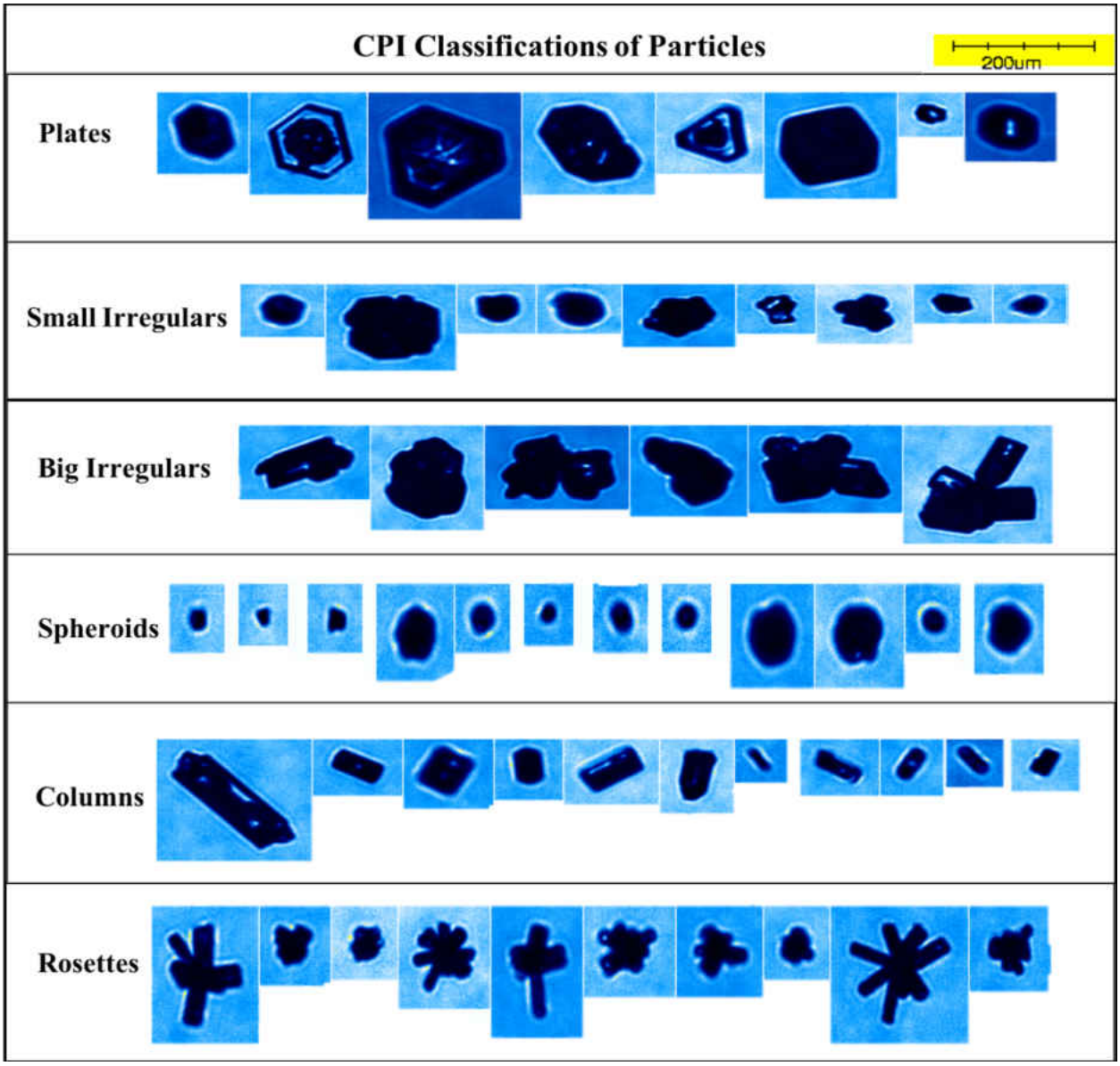

Figure 1: SPEC CPI imagery collected during 18 September 2013 flight from the SEAC[4]RS field campaign highlighting variations in crystal shape and size for plates, irregulars, spheroids, columns, rosettes.

Ice crystal microphysical properties have long been studied in laboratory and field experiments; however, large scale in-situ measurements are costly and in-situ cirrus retrievals are

unattainable on a global scale (Bailey and Hallett 2004; Lawson et al. 2019). The option of remote sensing has been explored in the past. For example, van Diedenhoven et al. (2012, 2013) developed a method for quantifying ice crystals into habit types by utilizing aspect ratio derived from airborne polarimeter observations. However, only broad plate-like or column-like categories can be derived using polarimeter observations alone. Noel et al. (2004) found lidar depolarization ratio to be sensitive to modeled aspect ratio which allowed for a coarse classification of habit types. Still only broad ice crystal categories including plates or spheroids, irregulars and columns were derived from the study. Also, distinguishing small from large ice crystals is a challenging task using lidar observations alone.

As suggested from previous studies ([‡]Bailey and Hallett 2009; [§]Noel et al. 2004; [*†]van Diedenhoven et al. 2012; [*†]van Diedenhoven et al. 2016) (Table 1), to retrieve detailed ice crystal information, combined lidar and polarimeter data, which includes aspect ratio, lidar depolarization ratio, asymmetry factor, effective radius and cloud temperature are needed. Those studies show that plate-like crystals with the lowest aspect ratios (<1) tend to have the highest asymmetry parameters (> 0.90) and are found at the warmest temperatures of the crystal habits (-20 to -40° C). Compact hexagonal crystals have the next lowest aspect ratio of approximately 1.0 but have depolarization ratios reaching 0.4. Rosettes have the next highest aspect ratio of approximately 2.0 and are found at colder temperatures (< -40° C). Due to variations in rosette development and number of branches, rosettes exhibit a range of depolarization ratios (0.25 to 0.50). Finally, columns tend toward the highest aspect ratios (>3.0) and largest depolarization ratios (>0.50) at cold cloud top temperatures (<-40° C). These findings are of general cirrus ice crystal characteristics; however, in reality, they would vary due to cirrus altitude and temperature, along with formation mechanism. To accomplish more detailed habit classifications and gain an

understanding of their properties, the combination of retrievals from lidar and polarimeter are necessary.

Table 2: Previously published values of aspect ratio, asymmtery factor, cloud temperature and depolarization ratio of various crystal habits (‡Bailey and Hallett 2009; §Noel et al. 2004; *†van Diedenhoven et al. 2012a; *†van Diedenhoven et al. 2016)

	Compact Hexagonal	Long Columns	Plates	Rosettes
Aspect Ratio *	~ 1.0	> 3.0	0.01 to 1.0	> 2.0
Asymmetry Factor†	0.70 to 0.80	0.80 to 0.90	0.90 to 0.95	0.80 to 0.90
Temperature ‡	-20 to -70 °C	-40 to -60 °C	-20 to -40 °C	-40 to -60 °C
Depolarization Ratio §	< 0.40	> 0.50	< 0.25	0.25 to 0.50

In this paper, collocated lidar and polarimeter observations of cirrus during the SEAC^{4}RS campaign are combined and analyzed using a K-means clustering technique. The results of the clustering are classified into seven ice crystal habits defined above. The classification technique is evaluated with in-situ data and frequencies of sampled habits from the remote sensing and in situ instruments are presented followed by an uncertainty analysis. This study is the first attempt to determine bulk ice crystal habit types using remote sensing data with the detail typical of in situ sensors. The ice particle habit results presented in this paper strengthen our understanding of cirrus cloud scattering parameters, while the classification method shown here can be used on other airborne remote sensing datasets and future space-based datasets to improve parameterizations of ice crystal habits and calculations of cirrus radiative forcing.

CHAPTER II

DATA

CPL

NASA's CPL is an elastic backscatter lidar providing multi-wavelength backscatter measurements of clouds and aerosols at 1064, 532, and 355 nm (McGill et al. 2002). Depolarization ratio, used to discriminate between liquid and ice clouds, is measured using the 1064 nm channel while cloud optical properties (i.e. extinction coefficient, ice water content) are retrieved from the 1064 and 532 nm channels, and aerosol discrimination utilizes the 532 and 355 nm channels (McGill et al. 2003). CPL has participated in over two dozen field campaigns since its first deployment in 2000 and serves as a reliable tool in the study of atmospheric profiling at high spatial and temporal resolutions. CPL raw data has a temporal resolution of 10 Hz and vertical resolution fixed at 30 m. The data is averaged to 1 s when creating data products, which equates to a 200 m horizontal resolution for an aircraft speed of 200 m/s. When mounted aboard NASA's ER-2 aircraft CPL points off-nadir by 2° due to the pitch of the aircraft. Therefore, the effect of horizontally oriented ice crystals on CPL data is negligible (Yorks et al 2011).

Once instrument corrections and calibration are applied to raw photon counts, CPL provides profiles of total attenuated backscatter (ATB) and the ratio of perpendicular to parallel backscatter (depolarization ratio) of clouds and aerosols (McGill et al. 2007). Level 2 algorithms use ATB profiles and depolarization ratio to further derive cirrus physical and optical properties. CPL level 2 algorithms categorize identified layers as ice clouds, liquid water clouds, or eight different aerosol types. A cloud phase (CP) algorithm is employed to discriminate between liquid

water clouds and ice clouds. High confidence ice clouds have a mid-layer temperature less than -20°C and a depolarization ratio greater than 0.25. Temperatures provided from MERRA-2 are interpolated to the CPL data and reported in the layer temperature product.

Five years of cloud optical properties from CPL were analyzed extensively by Yorks et al. (2011). A strong dependence of increasing layer volume depolarization ratio with decreasing temperature was found for all cirrus clouds. Statistics of ice cloud volume depolarization ratios and temperatures were explored to determine thresholds for cloud phase discrimination which are applied in this study. Previous research has also examined the sensitivity of lidar depolarization ratio to aspect ratio for modeled randomly oriented hexagonal ice crystals. Results show that depolarization ratio can be used to classify ice crystals into three categories: thin plates or spheroids, big and small irregulars and, columns with lowest uncertainties due to depolarization variability for columns (less than 4%), and generally less than the maximum of 15% for other habits (Noel et al. 2004). However, lidar alone does not provide sufficient information for a more detailed classification.

RSP

The RSP is a multi-channel, multi-angle airborne polarimeter with nine spectral channels in visible/near infrared and shortwave infrared bands providing measurements of total reflectance and polarized reflectance derived from the I, Q and U components of the Stokes vector. RSP scans along track over a ~120° angular range utilizing the fields of view of six boresighted refractive telescopes, which contribute to its 14 mrad field of view (similar to that of CPL). Each pixel is sampled at 152 viewing angles and 0.8° intervals (Cairns et al. 2003). When on board the NASA ER-2, the RSP's viewing angles drop to 134 usable angles (Sinclair et al. 2017). Ice-topped clouds

are selected by means of a liquid index derived from multi-angle polarimetry measurements around the 140° scattering angle, where liquid-topped clouds lead to a pronounced cloudbow feature (van Diedenhoven et al. 2012b). Clouds identified by RSP with a liquid index less than 0.3 and a cloud optical thickness greater than 5 are considered ice. The 1.59 μm and 2.25 μm channels are utilized in ice cloud retrievals for their sensitivity to ice/water discrimination.

RSP employs the first remote sensing method of retrieving ice crystal asymmetry parameter from multi-directional polarized measurements of aspect ratio and crystal distortion (van Diedenhoven et al. 2012a, 2013). RSP retrievals rely on individual hexagonal columns and plates to serve as proxies for more complex habit types (van Diedenhoven 2013). The asymmetry parameter values are determined by a closest fit to measured multi-directional polarized measurements from a look-up table consisting of randomly oriented hexagonal columns and plates with nearly continuous values of aspect ratio and crystal distortion levels (van Diedenhoven et al. 2012a). The distortion parameter (Macke et al. 1996) is a proxy for randomization of the crystal shape caused by a number of factors, such as large-scale crystal distortion and complexity, microscale surface roughness, and impurities within the crystals (Hong and Minnis, 2015; Liu et al., 2014; Neshyba et al., 2013). A definition of aspect ratio with an upper limit of unity for both columns and plates is used in this study (van Diedenhoven et al. 2016). Here aspect ratio is the ratio between dimensions of components of ice crystals. Given this definition, ice crystals must be specified as column-like or plate-like, as is standard for RSP ice cloud products. Once the crystal type is known the inverse of aspect ratio can be used to separate column-like crystals from their plate-like counterparts. Despite this separation, a finer habit classification is necessary for accurate representation of ice crystal shapes. Additionally, effective radius is retrieved at 1.59 and 2.25 microns, utilizing the 2.25 micron channel in this study for its ability to penetrate deeper into ice

clouds (van Diedenhoven et al. 2016b). RSP effective radius is ¾ the average ice volume divided by the average projected area (van Diedenhoven et al. 2016b). A look up table approach is used for effective radius retrievals that is described by van Diedenhoven et al. (2014, 2016). Note that, for each observation, an ice optical model is used for the effective radius retrievals that is consistent with the retrieved asymmetry parameter for that observation, as described by van Diedenhoven et al. (2014).

CPI

The SPEC Inc. CPI records high-resolution (2.3 micron pixel) digital images of individual ice cloud particles that pass through the sample volume of the imager (Lawson et al. 2001). Within each frame, CPI can record upwards of 25 particles simultaneously. The collected images are processed using SPEC Inc. software which derives crystal length, width, area and perimeter (Lawson and Baker 2006). These descriptors are then used to classify the ice crystals into seven habits: spheroid, column, plate, rosette, budding rosette, small irregular, and big irregular. A complete description of CPI classification criteria can be found in Appendix A of Lawson et al. (2006).

SEAC^{4}RS

Data from these instruments was collected during the NASA Studies of Emissions and Atmospheric Composition, Clouds and Climate Coupling by Regional Surveys (SEAC^{4}RS) campaign. SEAC^{4}RS took place in August and September 2013 and was based outside of Houston, Texas (Toon et al. 2016). During the campaign, 57 science flights were completed by NASA's ER-2 and DC-8 along with the SPEC Inc. Learjet spanning the continental United States and the

Gulf of Mexico. A large suite of remote sensing and in-situ instrumentation was implemented to study radiation, chemistry, and cloud microphysics. The CPL and RSP were both on board NASA's ER-2 for these flights, flying at a nominal altitude of 18-20 km (Sinclair et al. 2017). The following analysis consists of data from ten flights over the course of the campaign: August 2,6,21,27,30, September 4,11,13,18, 23. Continental and maritime cirrus were sampled during these flights, with special attention on 18 September flight where all three aircraft flew though a region of maritime convection (Toon et al. 2016).

CHAPTER III

METHODOLOGY

Ice Crystal Habit Definitions

The habit descriptions used in this study follow those put forth by Bailey and Hallett (2002, 2004, 2009) and Lawson et al. (2006), as also shown in Figure 1 using CPI imagery data collected on 18 September 2013 during the SEAC^{4}RS campaign. Here "plates" describes hexagons with a face width larger than height which results in an aspect ratio below unity. This category of crystals includes thick and thin plates along with asymmetric irregular plate-like crystals and is therefore not limited to pristine, symmetrical plates. "Columns" are hexagonal with a length greater than their face width resulting in aspect ratios greater than 1. Columns can be solid or hollow and short or long. It has been recently documented that an overemphasis of symmetric crystal habits exists, however these idealized shapes once found in habit diagrams are quite rare and the reality of defective and irregular crystals must be acknowledged (Bentley and Humphries 1931, Bailey and Hallett 2009). "Spheroids" are particles greater than 50 microns in diameter and appear spherical unless studied under close magnification. These are quasi-spherical compacted particles usually highly faceted and distorted. "Rosettes" presented in this study include budding rosettes which are not fully developed and general rosette-shaped particles which have multiple columnar structures gathered at a central point. Finally, "irregulars" are composed of compact faceted crystals which account for non-symmetric and defective crystals that do not fit into any of the above categories. Irregulars with aspect ratios less than 1 are categorized as plate-like irregulars, which consists of

a larger and smaller category, while those with aspect ratios larger than 1 are column-like irregulars which likely contain side planes.

Combined CPL-RSP Cirrus Retrievals

Two of the most promising instruments for ice crystal retrievals are active lidar and passive multi-angle polarimeters (van Diedenhoven 2018). Lidar's unique advantage to obtain vertical profiles of clouds allows for more detailed structure than passive or in situ sensors can provide on one overpass. Additionally, the sensitivity of lidar to optically thin layers allows for detections unattainable by cloud radars (Comstock et al. 2002). Multi-directional polarized measurements of varying ice crystal shapes provide information on the phase function and scattering of light by crystals using a minimum of three simultaneous observations. Thus, using collocated CPL and RSP data, a new method was developed for classifying ice crystal habit types from retrieved CPL-RSP observations in this study.

CPL-RSP Collocation

Coincident CPL and RSP observations were identified from the flights previously listed. These data were collocated temporally by synchronizing the time of overpasses for observations with the closest timestamps from both datasets. CPL and RSP were both mounted on the ER-2 and have similar sampling rates and fields of view so observations could be inter-compared. Despite these similarities, CPL and RSP have different sensitivities to cirrus clouds. For RSP cloud optical thickness greater than 5, the polarized reflectance does not depend on the optical thickness (Chepfer et al. 2001). However, for optical thicknesses less than 5 the cloud apparent optical thickness must be included in the look up table used for determining asymmetry parameter. The apparent optical thickness is determined by minimizing the difference between simulated and total

reflectance (van Diedenhoven 2012a). One of the advantages of including CPL for this study is its unique ability to measure optically thin cirrus layers (COD < 0.03) with high accuracy (McGill et al. 2002). CPL can also measure the vertical structure of cirrus which is not possible for CPI or passive sensors.

A ray-tracing simulation of light polarization as it interacts with hexagonal-based ice crystals is compared to retrieved CPL depolarization ratios of randomly oriented ice crystals in Noel et al. (2004). The depolarization ratio was found to be sensitive to the modeled aspect ratio which allowed for a coarse classification of ice crystals into three groups (and four habits) consisting of plates or spheroids with the lowest depolarization and aspect ratios, irregulars, and columnar crystals which are highly depolarizing and have larger aspect ratios. This comparison was recreated using CPL and RSP observations obtained during SEAC^{4}RS (see Figure 2) to observe the evolution of linear depolarization ratio with aspect ratio. To the authors' knowledge, this is the first confirmation that data from observations matches modeled data of the evolutions of depolarization ratio with increasing aspect ratio. Figure 2 demonstrates the relationship between depolarization ratio and aspect ratio, therefore it validates the use of combined lidar and polarimeter data to classify ice crystal habits.

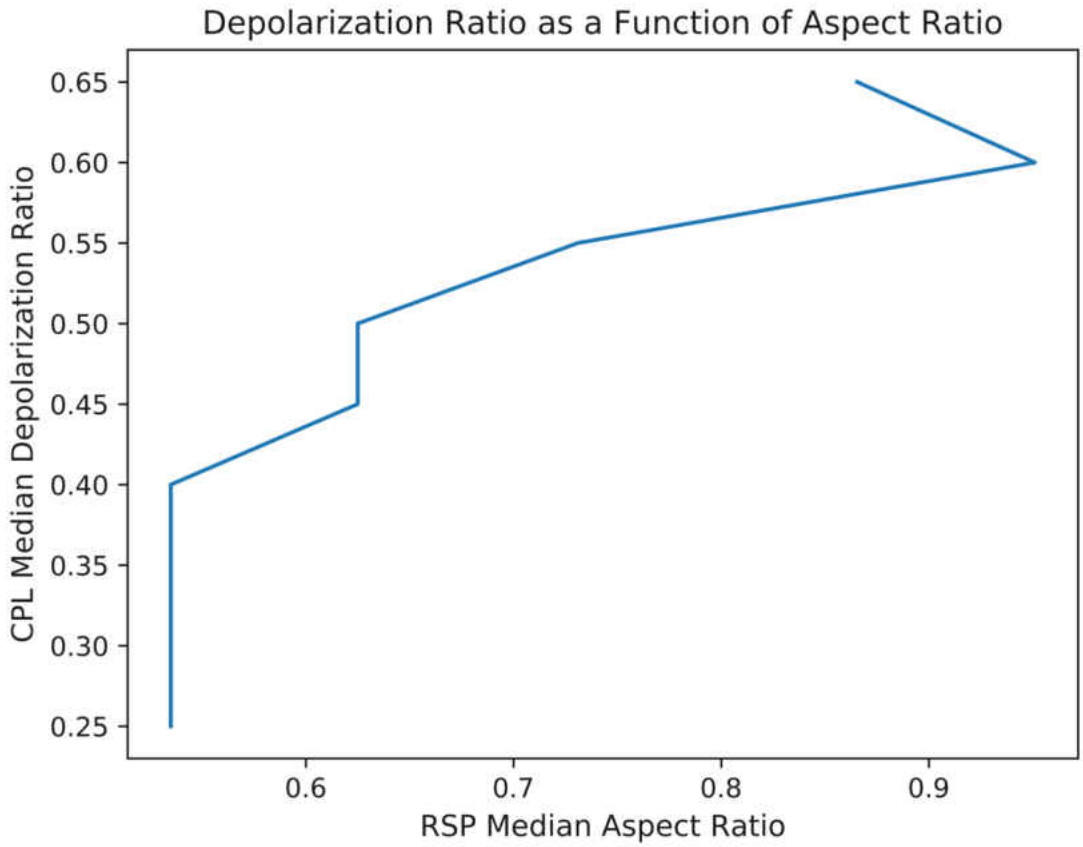

Figure 2: Evolution of depolarization ratio with aspect ratio for collocated lidar-polarimeter data obtained during the SEAC^{4}RS campaign.

The CPL properties investigated in this study are layer-integrated parameters, as such the results presented are bulk cloud top volume measurements of coincident lidar and polarimeter data. Conversely, the CPI records individual ice crystals that are detected and trigger the pulse of the imaging laser (Lawson et al. 2001). Therefore, it is assumed that the bulk volume measurements presented in this study are representative of the individual cirrus particle properties.

K-means based clustering analysis of ice crystal habit types

Thousands of seconds of ice crystal observations were identified in the collocated flight segments. Each observation made by CPL was additionally filtered in order to ensure that only ice clouds were being analyzed. Only cloud layers classified as cirrus by a cloud phase (CP) value of 3 were used. Additionally, these layers had to be colder than -25° C and have a depolarization ratio greater than 0.25. Due to the passive nature of RSP, only cloud top properties are retrieved and used in this study. Additionally, CPL signal attenuates before reaching cloud base for optically thick clouds. Therefore, results presented are for cloud tops of optically thick cirrus (COD >3.0). Once high confidence ice clouds classified from CPL and RSP were collocated and filtered, K-means clustering analysis was used to group ice crystals by the following features: depolarization ratio (CPL), aspect ratio (RSP), asymmetry parameter (RSP), effective radius (RSP), cloud-top temperature (CPL). RSP's crystal distortion retrievals were not use for clustering, since, for most cases, the maximum distortion level of 0.7 was retrieved during SEAC^{4}RS. The tendency to retrieve maximum distortion is consistent with previous findings using POLDER data (Hioki et al., 2016). However, we do report on statistics of distortion values for the different clusters. Seven initial cluster centers were selected to represent the habits identified by CPI. To distinguish between planar and columnar crystals initial clusters were separated based on aspect ratio. Clusters were assigned to data points with aspect ratios less than 1 which encompassed plates, plate-like irregulars and spheroids. Next, clusters were assigned to data points with aspect ratios greater than 1 which were made up of columns, column-like irregulars and rosettes. Through the iterative process each point in the normalized features was assigned to its closest cluster center and the seven cluster centers were updated to be the mean of the points within the cluster. The process terminates when the algorithm converges and there are no changes in cluster assignments.

Clustering was done for all SEAC^{4}RS cirrus observations and for the 18 September 2013 case study.

K-means was chosen for its efficiency in clustering several variables with many data points into a small number of known K values. Tighter clusters are produced from K-means than other clustering algorithms and data points are able to change cluster assignments as centroids are computed iteratively (Gan et al. 2007). K-means resulted in the classification of ice crystals habits into distinct clusters utilizing combined CPL and RSP observations for the first time.

CHAPTER IV

Results

The results of K-means clustering for each of the features listed above are presented in Figures 3 and 4 for the entire SEAC^{4}RS dataset. Two sets of clusters are presented: those for aspect ratios less than or greater than 1.0 (Figs 3 and 4, respectively). The clusters were assigned ice crystal habits based on their defining characteristics. Corresponding statistics for the clusters are summarized in Table 2.

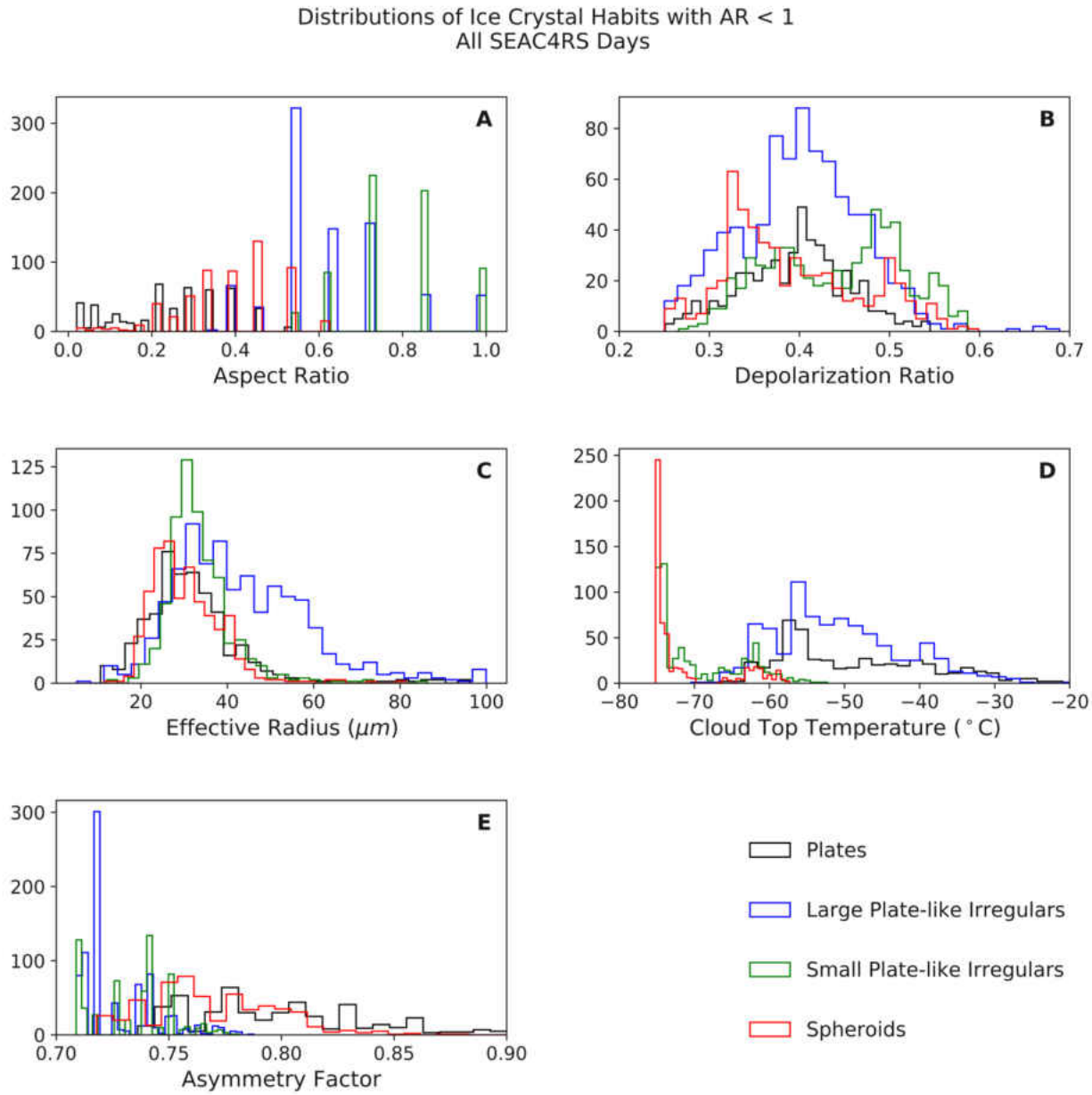

Figure 3- Distributions of collocated observations of plate-like ice crystal habits for aspect ratio (a), depolarization ratio (b), effective radius (c), cloud top temperature (d), and asymmetry factor (e) for all SEAC^{4}RS data.

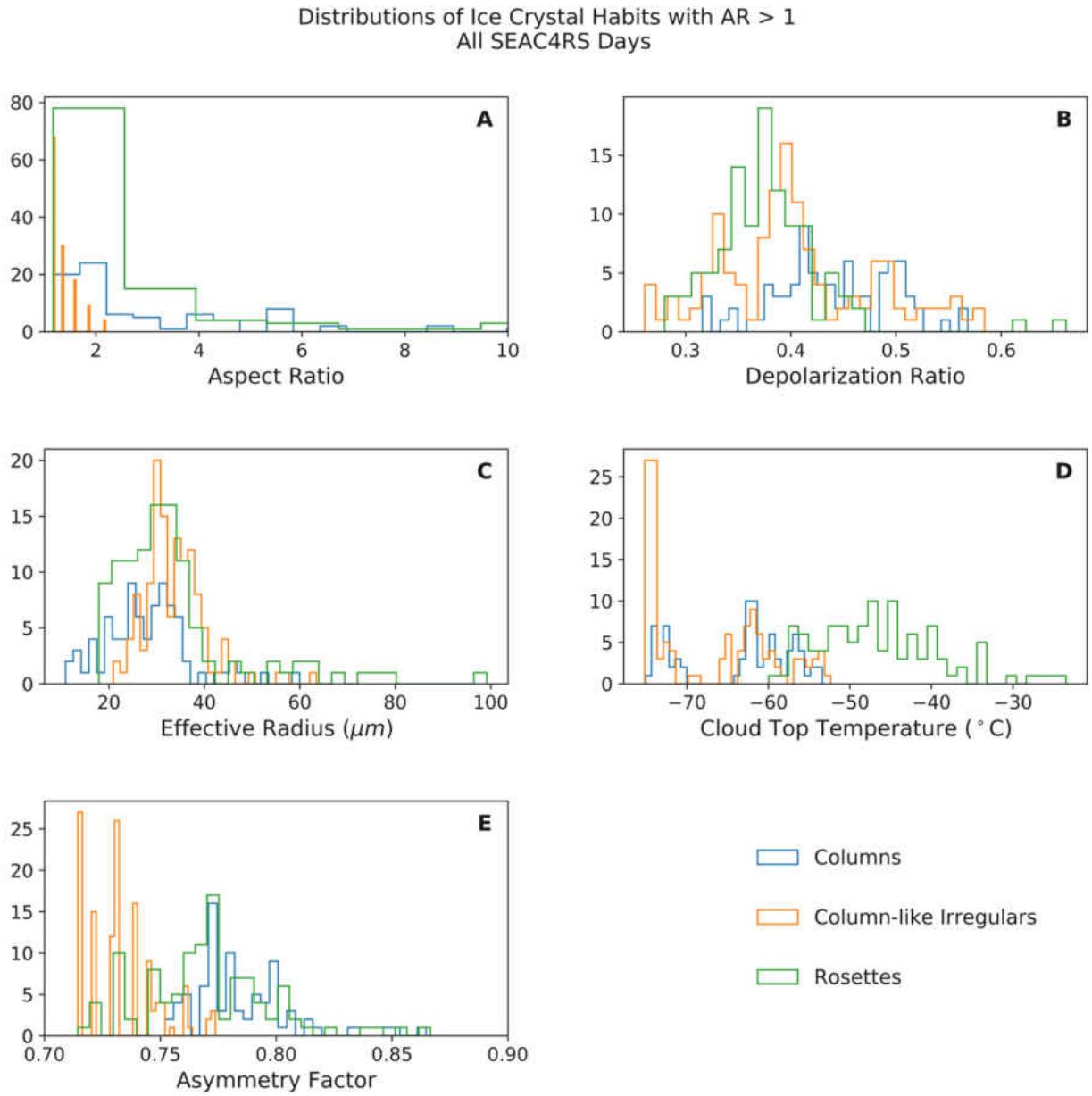

Figure 4- Distributions of collocated observations of column-like ice crystal habits for aspect ratio (a), depolarization ratio (b), effective radius (c), cloud top temperature (d), and asymmetry factor (e) for all SEAC^{4}RS data.

Table 2: Summary of CPL and RSP ice crystal habit statistics for the entire collocated SEAC^{4}RS dataset.

	Plates	Large Plate-like Irregulars	Small Plate-like Irregulars	Spheroids	Columns	Column-Like Irregulars	Rosettes
Samples	495	834	631	556	83	129	108
Mean Aspect Ratio	0.238	0.621	0.787	0.383	3.63	1.35	2.93
Median Aspect Ratio	0.245	0.535	0.731	0.391	2.18	1.17	1.870
Std dev Aspect Ratio	0.131	0.152	0.124	0.124	3.31	0.259	4.53
Mean Depolarization Ratio	0.394	0.400	0.440	0.392	0.441	0.404	0.377
Median Depolarization Ratio	0.399	0.402	0.447	0.373	0.438	0.395	0.374
Std dev Depolarization Ratio	0.059	0.067	0.073	0.075	0.056	0.074	0.054
Mean Effective Radius	31.86	43.21	33.47	30.57	28.03	33.83	33.54
Median Effective Radius	29.85	40.16	32.04	29.11	28.04	33.00	30.60
Std dev Effective Radius	12.15	15.64	7.67	8.31	9.04	6.54	14.18
Mean Cloud Top Temperature	-48.77	-50.72	-69.32	-71.42	-63.47	-67.41	-46.36
Median Cloud Top Temperature	-51.70	-51.69	-71.85	-74.30	-61.95	-71.65	-47.05
Std dev Cloud Top Temperature	10.05	8.64	5.78	5.38	6.55	7.39	7.61
Mean Asymmetry Factor	0.800	0.727	0.733	0.769	0.786	0.733	0.769
Median Asymmetry Factor	0.793	0.718	0.740	0.767	0.781	0.731	0.768
Std dev Asymmetry Factor	0.043	0.016	0.017	0.029	0.023	0.015	0.028
Mean Distortion	0.577	0.659	0.616	0.586	0.558	0.656	0.589
Median Distortion	0.700	0.700	0.600	0.650	0.600	0.700	0.600
Std Dev Distortion	0.199	0.075	0.079	0.148	0.023	0.062	0.098

Plates were categorized as the cluster with the lowest mean aspect ratio (0.24) and highest mean asymmetry factor (0.80). These are typical characteristics of plates and have been previously reported (see Table 1). As previously noted, the definition of plates is not limited to symmetric, ideal hexagonal plates. In this study, the plate category includes thick, thin and asymmetric polycrystalline plate-like crystals; samples of which are shown in Fig. 1. Thin plates have the highest asymmetry factors with values surpassing 0.9, while thicker plates or aggregates of plates tend toward lower values of 0.73. Plates also have relatively warm cloud top temperatures, within this dataset with a mean cloud top temperature of -48° C. It is expected that plates have warmer temperatures than columnar crystals based on previous findings summarized in Table 1.

At the very coldest temperatures, with a mean value of -71° C, small compact particles are found. At these temperatures it is likely that the particles are barely developed budding rosettes, small columnar crystals and irregular polycrystals (Bailey and Hallett 2009). This cluster is classified as spheroids; however, it should not be assumed that the particles are spheres; rather that they are distorted, spherical crystals that may be still developing into a distinct habit.

The remaining clusters with aspect ratios less than unity are classified as irregulars within the plate-like regime. Irregulars within this regime were separated into two groups to further differentiate habits based on size: large and small plate-like irregulars. The first group of irregulars have a mean aspect ratio of 0.62. This group is warmer (mean temperature of -50° C) and larger (mean radius of 43 microns) than the second cluster of irregulars. The colder and smaller group of irregulars with a mean cloud top temperature of -69° C and effective radius of 33 microns, has a higher aspect ratio of 0.78 due to a larger deviation from symmetry than the first group of irregulars. Both irregular clusters have asymmetry factors of approximately 0.73 suggesting dense crystals or distorted aggregates of crystals. High mean depolarization ratios of 0.40 and 0.44,

respectively, confirm the irregular nature of these clusters. Irregulars also have the largest effective radii of clusters analyzed with aspect ratios less than unity with mean values of 43- and 33-microns. Interestingly, the average distortion parameter of the irregulars is greater than that of plates, although the distortion parameter was not part of the clustering procedure. This is consistent with greater crystal complexity for irregulars than for plates. A large cloud top temperature difference exists between the two irregular clusters. The smaller irregular cluster has minimum temperatures reaching -75°C while the larger irregular cluster has minimum temperatures nearly 15°C warmer. These temperature differences suggest the second cluster contains more compact crystals while those in the first group are thin. This is confirmed by the peak in lower asymmetry factors for the second group of irregulars (e.g. Table 2).

Distributions of ice crystal habits with aspect ratios greater than 1.0 for SEAC^{4}RS are shown in Figure 4. Rosettes and columns typically have aspect ratios greater than unity and can exceed aspect ratios of four (Bailey and Hallett 2009). In this dataset, the cluster with largest mean aspect ratios (2.63) and highest mean depolarization ratio (0.44) was identified as columns. These values agree with those listed in Table 1 which were found in previous studies. Additionally, column temperatures fit well within the known column temperature regime which is colder than -40° C. Overall temperatures for the dataset are colder than previously published findings (Table 1). This is due to the high altitude at which cloud top temperatures are retrieved as opposed to lower altitude in situ measurements. Columns with mean temperatures of -63° C suggest they are found near cloud top where in situ measurements are difficult to obtain.

Rosettes also have high aspect ratios with values increasing as the number of attached branches increases (Um et al., 2015). Therefore, the group with the second highest mean aspect ratio (2.93) is categorized as rosettes. The associated standard deviation of rosettes is large due to

the varying stages of development of the crystals and their branches. Rosettes fall within the expected temperature range (-30° to -40° C) reported by Bailey and Hallett (2009). Those found in warmer regions transition to grow in width and can contain side planes or hollow branches, while rosettes found in the colder temperatures have more distinct branches intersecting the central core. At the coldest temperatures (< -50°C), there is a retardation in bullet growth and crystals are small and compact. These temperatures match those found by Lawson et al. (2010) for results in cirrus. Rosettes depolarization ratios are lower than columns (0.37 v 0.44) as is expected based on values of depolarization ratio reported by Noel et al. (2004).

The final cluster of crystals are identified as column-like irregulars. Although they are within the column regime, the mean aspect ratio of this group (1.35) is lower than that of columns or rosettes. The mean asymmetry factor (0.73) is also lower than that of other habits with aspect ratios greater than one. As also seen for the plate-like regime, the average distortion parameter of the column-like irregulars is greater than that of columns, consistent with their greater complexity.

The frequency of each assigned habit classification for the collocated CPL-RSP data during all of the SEAC^{4}RS campaign is presented in Figure 5. Irregulars with low aspect ratios dominate the dataset with a frequency of 52% followed by spheroids (20.5%), plates (16%), columns and column-like irregulars (7.5%), and rosettes (3.7%). These results compare favorably with those previously found by Noel et al. (2004) in which CPL and CPI data was analyzed from the CRYSTAL-FACE field campaign. The habits found in convective anvils sampled by Noel et al. (2004) were dominated by irregulars (~ 60%), followed by plates and spheroids (34%) and columns (6%). Crystals could only be categorized into broad groups comprised of plates/spheroids, irregulars, and columns based on depolarization and aspect ratio. Because lidar depolarization ratio is not a function of particle size or particle asymmetry, no distinctions could be made between

large and small crystals or rosettes and columns which both have aspect ratios greater than unity. Most of the SEAC[4]RS data sampled tropical anvil cirrus over the Gulf of Mexico, with 75% of data falling at a latitude between 19.11 to 27.56° N and longitude 124.2 to 92.4° W. The findings presented also compare favorably with those of Lawson et al. (2010) in which tropical anvil cirrus were sampled. Lawson et al. (2010) reported that fresh anvils rarely contain rosettes, but instead were comprised mostly of irregulars. These results highlight the agreement in current and previous findings and showcase the utility of a combined remote sensing retrieval technique for ice crystal classifications.

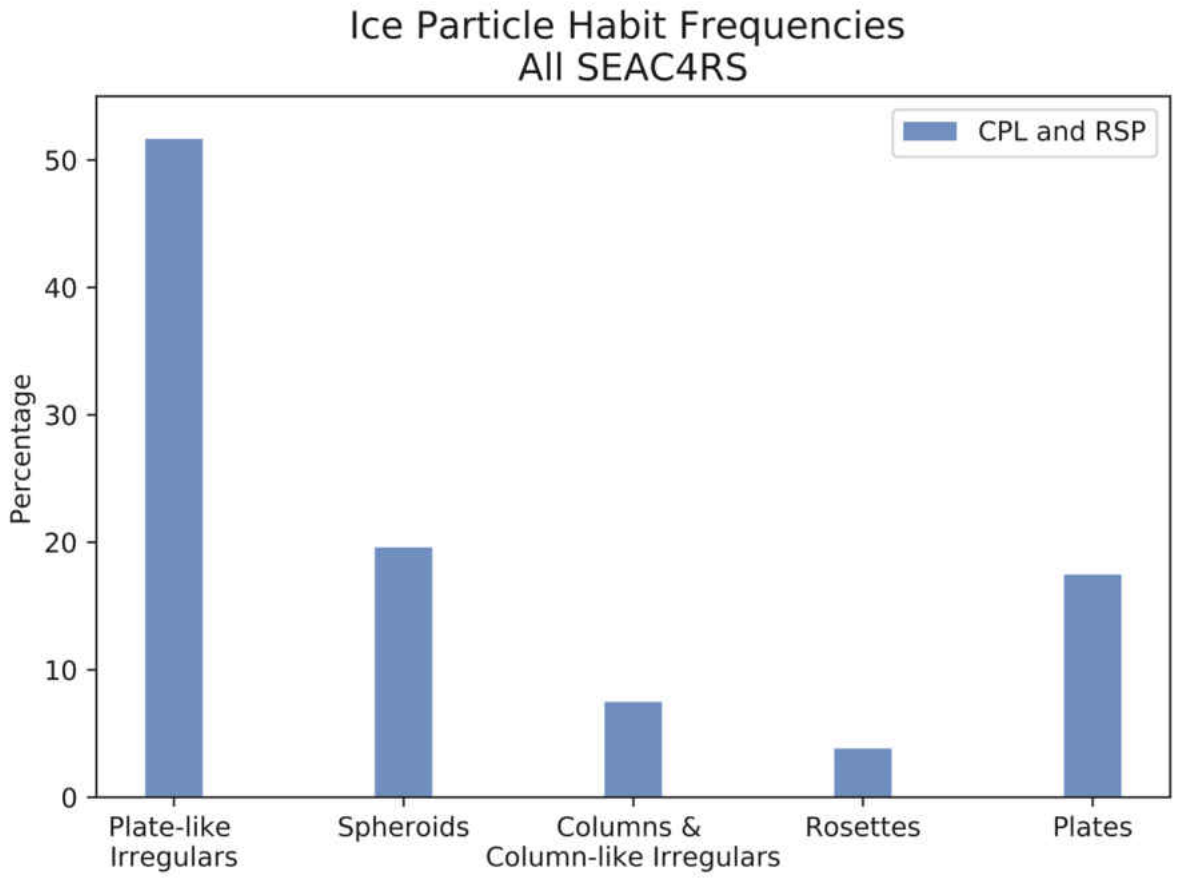

Figure 5: Frequencies of ice crystal habits for all collocated SEAC[4]RS data dominated by plate-like irregulars (52%), followed by spheroids (20.5%), plates (16%), columns and column-like irregulars (7.5%), and rosettes (3.7%).

CHAPTER V

VALIDATION AND UNCERTAINTY

The previously described analysis was applied to the case study date of 18 September 2013 to classify ice crystals sampled in anvil cirrus into habit types. SPEC CPI habit classifications were compared to classifications made using the combined CPL and RSP retrieval method. To the authors' knowledge, this is the only flight day of nearly coincident CPL, RSP, and CPI observations from the SEAC^{4}RS campaign. The results of this comparison are shown in Figure 6. In both cases irregulars with low aspect ratios comprised over half of all observations. Also, comparisons for both retrieval methods agree within 5% in frequency for plate-like irregulars, spheroids, columns and column-like irregulars and rosettes. The least observed habit for the combined retrieval technique was rosettes; however, the least observed habit from CPI was plates which comprised only 0.4% of observations. A source of the disagreement stems from differences in habit classification definitions. The definition of plates in this study does not limit crystals only to symmetric plates so this category likely includes irregulars. Sampling differences also attribute to the disagreement. While CPI captures individual particles, CPL and RSP sample bulk cloud properties. Additionally, the measurements from CPL-RSP and CPI are not exactly coincident. Both CPL and RSP were mounted on board the ER-2 while CPI was on the Learjet. These two aircraft never flew in a stacked alignment with the ER-2 above the Learjet, but rather sampled the same clouds at slightly different times. The CPI data collected during the 18 September flight

segment was at a mean altitude of 7.0 km and mean temperature of -18.5° C, while CPL-RSP data was collected at a mean altitude of 11.4 km and mean temperature of -59.6° C. Thus, the comparison is not "apples to apples" but we assume there is little cloud evolution over the minutes of sampling difference so that the CPI data is representative of the bulk cloud top retrievals by the lidar and polarimeter. To the authors' knowledge, there are no existing datasets that include exactly coincident lidar, polarimeter, and cloud probe imagery to complete a more "apples to apples" study.

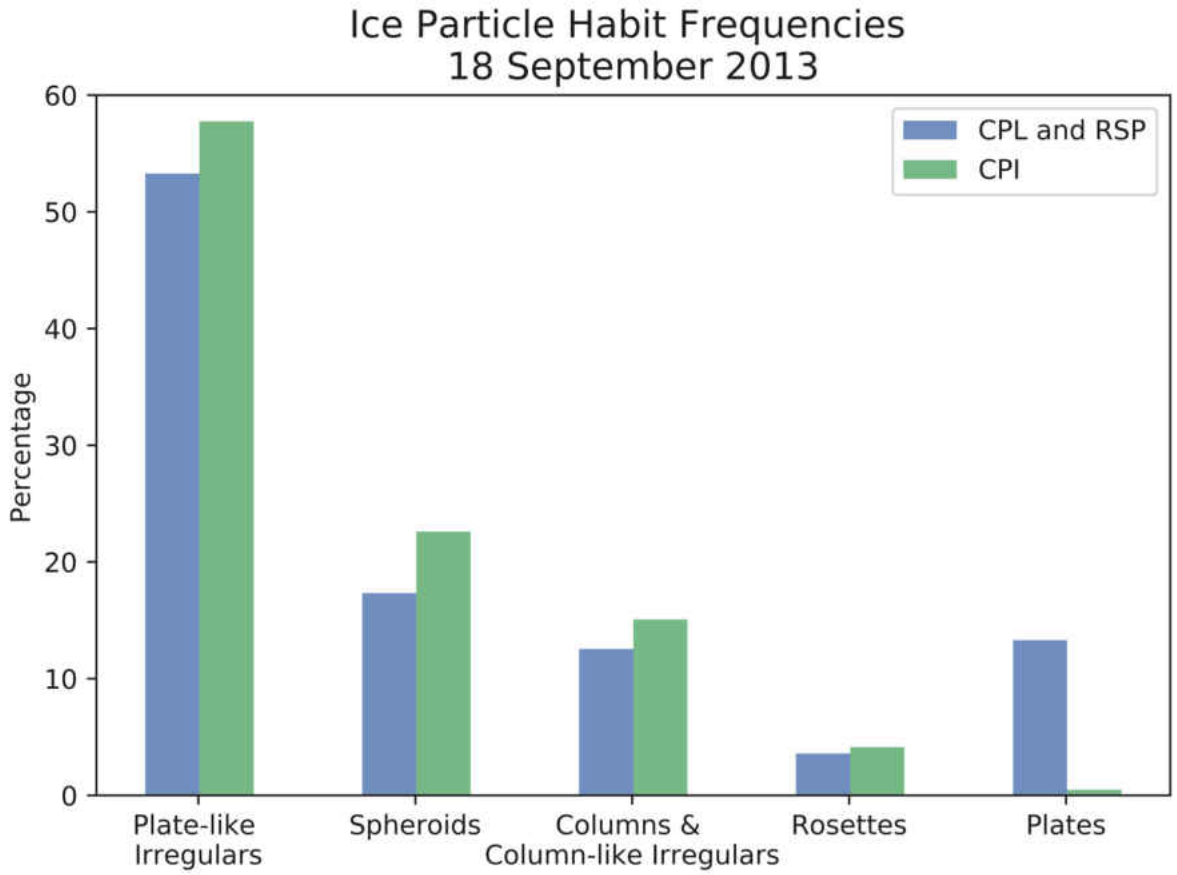

Figure 6: Frequencies of ice crystal habits classified by SPEC CPI (green) and the newly developed CPL-RSP technique (blue) for a case study on 18 September 2013 from the SEAC^{4}RS campaign. Agreement for irregulars, spheroids, columns and rosettes is within 5% with less agreement for plates (~16%)

To quantify the uncertainty in the presented analysis, the importance of each attribute used in the classification was assessed. To do this, the K-means technique was repeated five times, each time removing one of the following parameters: aspect ratio, depolarization ratio, cloud top temperature, asymmetry factor, and effective radius. The resulting clusters were classified into seven habits, just as before. The frequencies of habit types were compared to the frequencies when all five attributes were present in the analysis. Differences in frequencies were attributed to the parameter that was eliminated in that particular trial. For each habit, the differences in frequencies due to removing an attribute were summed. The change in frequency due to each attribute was divided by the sum and this percent was used as the weight. Table 3 summarizes the weights for each attribute used in the habit classification. Whichever missing parameter caused the largest change in frequency was deemed the most important. This analysis provided weights which could be applied to the corresponding attributes.

Table 3: Weights of individual attributes used to calculate overall uncertainty in each habit type.

	Aspect Ratio	Depolarization Ratio	Cloud Top Temperature	Asymmetry Factor	Effective Radius
Plates	0.08	0.045	0.47	0.35	0.049
Large Plate-like Irregulars	0.34	0.03	0.23	0.26	0.11
Small Plate-like Irregulars	0.23	0.05	0.28	0.21	0.22
Spheroids	0.43	0.06	0.25	0.17	0.08
Columns	0.07	0.13	0.30	0.40	0.02
Column-like Irregulars	0.1	0.02	0.10	0.50	0.27
Rosettes	0.10	0.20	0.30	0.13	0.21

Once an appropriate weight was established for each parameter in the classification, the uncertainty of a cluster from each attribute is computed by dividing the normalized variance in

each attribute for a cluster by the normalized values of that attribute, then multiplied with the corresponding weight as defined in Table 3. The overall uncertainty for a cluster is thus computed by summing computed uncertainties from all used attributes for that cluster, as suggested in Equation 1.

$$\Delta c = \frac{\partial c}{\partial T}\Delta T + \frac{\partial c}{\partial dp}\Delta dp + \frac{\partial c}{\partial AR}\Delta AR + \frac{\partial c}{\partial g}\Delta g + \frac{\partial c}{\partial r}\Delta r \quad (5.1)$$

Here ΔC is the relative uncertainty of the classification method. The derivative terms are the uncertainties in the classification method due to various parameters and are tabulated in Table 3. ΔT, Δdp, ΔAR, Δg and Δr are the relative uncertainties in temperature, depolarization, aspect ratio, asymmetry factor and effective radius respectively. The overall uncertainty is computed based on Equation 1 and is listed in Table 4 for each habit. As expected, columns and plates have the lowest uncertainty of 9.7% and 11.3%, respectively. These habits are the most distinct and would have higher confidence classifications than other habits. Rosettes have the next lowest uncertainty with 20.1%. Fully developed rosettes will be easily distinguished from other habits, while budding rosettes are more likely to be misclassified. The irregular habits have higher uncertainties (29.4, 45.4, and 23.2 %), as expected. Those groups contain fewer distinctions to separate them from others and likely contain a mix of asymmetric, non-pristine crystals. Relative layer-integrated depolarization ratio uncertainties from CPL are reported as <10% (Yorks et al. 2011) while van Diedenhoven et al. (2012a) and van Diedenhoven et al. (2016) report RSP relative uncertainties for aspect ratio (20%), effective radius (15%) and asymmetry parameter (5%). Overall, the uncertainties presented are reasonable given the high-quality aircraft data used in the analysis. For potential space-based applications of this classification method, higher uncertainties would be expected.

Table 4: Overall uncertainties calculated for each crystal habit type with lowest uncertainty for distinct habits (plates, columns, rosettes) and greater uncertainty for irregular crystals.

	Plates	Large Plate-like Irregulars	Small Plate-like Irregulars	Spheroids	Columns	Column-like Irregulars	Rosettes
Overall Uncertainty	11.3%	29.4%	45.4%	44.1%	9.7%	23.2%	20.1%

CHAPTER VI

CONCLUSIONS

By combining CPL and RSP cirrus cloud observations during the SEAC^{4}RS campaign, a K-means clustering technique was applied to classify optically-thick cloud top ice crystals into seven habit types. This technique demonstrates a finer classification than what is possible from lidar or polarimeter alone. It was determined that the most critical parameters for determining habit type are aspect ratio and cloud temperature, followed by depolarization ratio, asymmetry factor, and effective radius. The results of this classification were compared to in-situ CPI data and frequencies for irregulars, spheroids, columns and rosettes agreed within 5%, while less agreement was found for plates (~16%). The relationship between depolarization ratio and aspect ratio modeled by Noel et al. (2004) was successfully recreated using the combined CPL-RSP retrievals. While previous research showed a classification of ice crystals into 3 broad categories based on depolarization ratio, the present classification can be expanded to 7 categories. Additionally, the high frequency of irregulars and spheroids in contrast to the relatively low number of observations of rosettes agrees well with the findings presented in Lawson et al. (2010) for similar anvil cirrus. These findings are expected to agree with those of Lawson et al. (2010) because in both studies, mostly fresh anvil still attached to convection were analyzed.

While radiative forcing models currently assume an oversimplified crystal classification of plates and columns, this unique dataset provides insights of ice crystal parameters for more detailed

habit types. For the first time, lidar and polarimeter data is combined to provide valuable insight of microphysical ice crystal properties useful for model simulations and the ongoing investigation of radiative impacts of cirrus. Although depolarization ratio can be used for coarse habit classification, additional parameters such as aspect ratio and asymmetry factor provide information that is necessary for a finer classification.

The presented technique may be applied to combined measurements of the CALIOP lidar and POLDER instrument (van Diedenhoven et al. 2014b), which were both in NASA's A-Train constellation. Combined backscatter lidar and a multi-channel/polarization imager flown on board the same platform serves as a direct response to priorities set forth by NASA's Decadal Strategy for Earth Observation from Space (2018). The Aerosols, Clouds, Convection, and Precipitation (A-CCP) spaceborne mission also calls for combined lidar and polarimeter observations to study cloud and aerosol properties. The usefulness of a combined retrieval method is extensive, however there is a dearth of coincident flights available for this type of analysis. Additional coincident observations from lidar, polarimeter, and in situ instrumentation are necessary for finer habit classifications and parameterizations in radiative forcing models, and to improve the technique of habit classification using remote sensing data shown here.

APPENDICES

Appendix A
List of Abbreviations

Table 5: List of Abbreviations

Abbreviation	Full Text
A-CCP	The Aerosols, Clouds, Convection, and Precipitation
ATB	Attenuated total backscatter
CALIPSO	The Cloud-Aerosol Lidar and Infrared Pathfinder Satellite Observation
COD	Cloud optical depth
CP	Cloud phase
CPI	Cloud Particle Imager
CPL	Cloud Physics Lidar
NASA	National Aeronautics and Space Administration
POLDER	Polarization and Directionality of the Earth's Reflectances
RSP	Research Scanning Polarimeter
Seac4rs	Studies of Emissions and Atmospheric Composition, Clouds and Climate Coupling by Regional Surveys

REFERENCES

Bailey, M., and J. Hallett, 2002: Nucleation effects on the habit of vapour grown ice crystals from −18° to −42°C. Quart. J. Roy. Meteor. Soc., 128, 1461–1483.

Bailey, M., and J. Hallett, 2004: Growth rates and habits of ice crystals between −20° and −70°C. J. Atmos. Sci., 61, 514–554.

Bailey, M. P., and J. Hallett, 2009: A comprehensive habit diagram for atmospheric ice crystals: Confirmation from the laboratory, AIRS II, and other field studies. J. Atmos. Sci., 66, 2888–2899.

Baker BA, Lawson RP (2006) In situ observations of the microphysical properties of wave, cirrus and anvil clouds. Part 1: Wave clouds. J Atmos Sci 63:3160–3185

Bentley, W. A., and W. J. Humphreys, 1931: Snow Crystals. McGraw-Hill, 226 pp.

Brian Cairns, Edgar E. Russell, Joseph D. LaVeigne, and Philip M. W. Tennant "Research scanning polarimeter and airborne usage for remote sensing of aerosols", Proc. SPIE 5158, Polarization Science and Remote Sensing,(12December2003); https://doi.org/10.1117/12.518320

Campbell, J. R., Vaughan, M. A., Oo, M., Holz, R. E., Lewis, J. R., and Welton, E. J.: Distinguishing cirrus cloud presence in autonomous lidar measurements, Atmos. Meas. Tech., 8, 435–449, https://doi.org/10.5194/amt-8-435-2015, 2015.

Chepfer, H., P. Goloub, J. Riedi, J. F. de Haan, and J. W. Hovenier, 2001: Ice crystal shapes in cirrus clouds derived from POLDER-1/ADEOS-1. J. Geophys. Res., 106, 7955–7966.

Comstock, J. M., T. P. Ackerman, and G. G. Mace (2002), Ground-based lidar and radar remote sensing of tropical cirrus clouds at Nauru Island: Cloud statistics and radiative impacts, J. Geophys. Res., 107(D23), 4714, doi:10.1029/2002JD002203.

Gan, G., Ma, C., and Wu, J. 2007. Data Clustering: Theory, Algorithms, and Applications. ASA-SIAM Series on Statistics and Applied Probability. SIAM.

Holz, R. E., Platnick, S., Meyer, K., Vaughan, M., Heidinger, A., Yang, P., Wind, G., Dutcher, S., Ackerman, S., Amarasinghe, N., Nagle, F., and Wang, C.: Resolving ice cloud optical thickness biases between CALIOP and MODIS using infrared retrievals, Atmos. Chem. Phys., 16, 5075–5090, https://doi.org/10.5194/acp-16-5075-2016, 2016.

Hioki, S., P. Yang, B. A. Baum, S. Platnick, K. G. Meyer, M. D. King, and J. Riedi (2016), Degree of ice particle surface roughness inferred from polarimetric observations, *Atm. Chem.Phys.*, *16*(12), 7545–7558, doi:10.5194/acp-16-7545-2016.

Hong, G., and P. Minnis (2015), Effects of spherical inclusions on scattering properties of small ice cloud particles, *J. Geophys. Res.*, *120*(7), 2951–2969, doi:10.1002/2014JD022494

Lawson RP, Baker BA, Schmitt CG, Jensen TL (2001) An overview of microphysical properties of Arctic clouds observed in May and July 1998 during FIRE ACE. J Geophys Res 106 (14):989–15014. https://doi.org/10.1029/2000JD900789

Lawson, R. P., B. A. Baker, C. G. Schmitt, and T. L. Jensen, 2001: An overview of microphysical properties of Arctic clouds observed in May and July during FIRE.ACE. J. Geophys. Res., 106, 14989–15014.

Lawson RP, Baker B, Pilson B, Mo Q (2006) In situ observations of the microphysical properties of wave, cirrus, and anvil clouds. Part II: cirrus clouds. J Atmos Sci 63:3186. https://doi.org/10. 1175/JAS3803.1

Lawson, R. P., E. J. Jensen, D. L. Mitchell, B. Baker, Q. Mo,
and B. Pilson, 2010: Microphysical and radiative properties of tropical clouds investigated in TC4 and NAMMA. J. Geophys. Res., 115, D00J08, doi:https://doi.org/10.1029/2009JD013017.

Lawson, R., Woods, S., Jensen, E., Erfani, E., Gurganus, C., Gallagher, M., Connolly, P., Whiteway, J., Baran, A., May, P., Heymsfield, A., Schmitt, C., McFarquhar, G., Um, J., Protat, A., Bailey, M., Lance, S., Muehlbauer, A., Stith, J., Korolev, A., Toon, O.B., and Krämer, M. (2019) A review of ice particle shapes in cirrus formed in situ and in anvils. *Journal of Geophysical Research:Atmospheres*, **124**, 10049– 10090. https://doi.org/10.1029/2018JD030122

Liu, C., R. L. Panetta, and P. Yang (2014), The effective equivalence of geometric irregularity and surface roughness in determining particle single-scattering properties., *Optics express*, *22*(19), 23620–7, doi:10.1364/OE.22.023620.

Macke, A., J. Mueller, and E. Raschke (1996), Single scattering properties of atmospheric ice crystals, *J. Atmos. Sci.*, *53*(19), 2813–2825.

McGill, M. J., D. L. Hlavka, W. D. Hart, V. S. Scott, J. D. Spinhirne, and B. Schmid (2002), The Cloud Physics Lidar: Instrument description and initial measurement results, Appl. Opt., 41, 3725–3734, doi:10.1364/AO.41.003725.

McGill, M. J., D. L. Hlavka, W. D. Hart, E. J. Welton, and J. R. Campbell (2003), Airborne lidar measurements of aerosol optical properties during SAFARI-2000, J. Geophys. Res., 108(D13), 8493, doi:10.1029/2002JD002370.

McGill, M. J., M. A. Vaughan, C. R. Trepte, W. D. Hart, D. L. Hlavka, D. M. Winker, and R. Kuehn (2007), Airborne validation of spatial properties measured by the CALIPSO lidar, J. Geophys. Res., 112, D20201, doi:10.1029/2007JD008768.

Neshyba, S. P., B. Lowen, M. Benning, A. Lawson, and P. M. Rowe (2013), Roughness metrics of prismatic facets of ice, *J. Geophys. Res.*, *118*(8), 3309–3318, doi:10.1002/jgrd.50357.

Noel, V., D. M. Winker, M. McGill, and P. Lawson (2004), Classification of particle shapes from lidar depolarization ratio in convective ice clouds compared to in situ observations during CRYSTAL-FACE, J. Geophys. Res., 109, D24213, doi:10.1029/2004JD004883.

[online] Available: https://science.nasa.gov/earth-science/decadal-survey.

Sinclair K, van Diedenhoven B, Cairns B, Yorks J, Wasilewski A, McGill M (2017) Remote sensing of multiple cloud layer heights using multi-angular measurements. Atmos Meas Tech 10:2361-2375. https://doi.org/10.5194/amt-10-2361-2017

Toon, O. B., et al. (2016), Planning, implementation and scientific goals of the Studies of Emissions and Atmospheric Composition, Clouds and Climate Coupling by Regional Surveys (SEAC^{4}RS) field mission, J. Geophys. Res. Atmos., 121, 4967– 5009, doi:10.1002/2015JD024297.

Um, J., G. M. McFarquhar, Y. P. Hong, S.-S. Lee, C. H. Jung, R. P. Lawson, and Q. Mo, 2015: Dimensions and aspect ratios of natural ice crystals. Atmos. Chem. Phys., 15, 3933–3956, doi:https://doi.org/10.5194/acp-15-3933-2015.

van Diedenhoven, B., B. Cairns, I. V. Geogdzhayev, A. M. Fridlind, A. S. Ackerman, P. Yang, and B. A. Baum, 2012: Remote Sensing of ice crystal asymmetry parameter using multi-directional polarization measurements—Part 1: Methodology and evaluation with simulated measurements. Atmos. Meas. Tech., 5, 2361–2374.

van Diedenhoven, B., A.M. Fridlind, A.S. Ackerman, and B. Cairns, 2012: Evaluation of hydrometeor phase and ice properties in cloud-resolving model simulations of tropical deep convection using radiance and polarization measurements. *J. Atmos. Sci.*, **69**, 3290-3314, doi:10.1175/JAS-D-11-0314.1.

van Diedenhoven, B., B. Cairns, A. M. Fridlind, A. S. Ackerman, and T. J. Garrett, 2013: Remote sensing of ice crystal asymmetry parameter using multi-directional polarization measurements-Part 2: Application to the Research Scanning Polarimeter. Atmos. Chem. Phys., 13, 3185–3203.

van Diedenhoven, B., A.M. Fridlind, B. Cairns, and A.S. Ackerman, 2014: Variation of ice crystal size, shape and asymmetry parameter in tops of tropical deep convective clouds. *J. Geophys. Res. Atmos.*, **119**, no. 20, 11809-11825, doi:10.1002/2014JD022385

van Diedenhoven, B., A. S. Ackerman, A. M. Fridlind, and B. Cairns (2016), On averaging aspect ratios and distortion parameters over ice crystal population ensembles for estimating effective scattering asymmetry parameters, J. Atmos. Sci., 73(2), 775–787.

van Diedenhoven, B., A.M. Fridlind, B. Cairns, A.S. Ackerman, and J. Yorks, 2016: Vertical variation of ice particle size in convective cloud tops. *Geophys. Res. Lett.*, **43**, no. 9, 4586-4593, doi:10.1002/2016GL068548

van Diedenhoven, B. (2018). Remote Sensing of Crystal Shapes in Ice Clouds. In Light Scattering, Radiative Transfer and Remote Sensing, pages 197–250.

Yorks, J. E., D. L. Hlavka, W. D. Hart, and M. J. McGill, 2011: Statistics of cloud optical properties from airborne lidar measurements. J. Atmos. Oceanic Technol., 28, 869–883.

Wendisch, M., P. Pilewskie, J. Pommier, S. Howard, P. Yang, A. J. Heymsfield, C. G. Schmitt, D. Baumgardner, and B. Mayer, 2005: Impact of cirrus crystal shape on solar spectral irradiance: A case study for subtropical cirrus. J. Geophys. Res., 110, D03202, doi:10.1029/2004JD005294.

Zhang, Y., A. Macke, and F. Albers, 1999: Effect of crystal size spectrum and crystal shape on stratiform cirrus radiative forcing. J. Atmos. Res., 52, 59–75.